HHS Public Access

Author manuscript

Phys Med Biol. Author manuscript; available in PMC 2017 March 07.

Published in final edited form as:

Phys Med Biol. 2016 March 7; 61(5): N193–N202. doi:10.1088/0031-9155/61/5/N193.

On the assessment of spatial resolution of PET systems with iterative image reconstruction

Kuang Gong, **Simon R Cherry**, and **Jinyi Qi**

Department of Biomedical Engineering, University of California, Davis, CA, USA

Abstract

Spatial resolution is an important metric for performance characterization in PET systems. Measuring spatial resolution is straightforward with a linear reconstruction algorithm, such as filtered backprojection, and can be performed by reconstructing a point source scan and calculating the full-width-at-half-maximum (FWHM) along the principal directions. With the widespread adoption of iterative reconstruction methods, it is desirable to quantify the spatial resolution using an iterative reconstruction algorithm. However, the task can be difficult because the reconstruction algorithms are nonlinear and the non-negativity constraint can artificially enhance the apparent spatial resolution if a point source image is reconstructed without any background. Thus, it was recommended that a background should be added to the point source data before reconstruction for resolution measurement. However, there has been no detailed study on the effect of the point source contrast on the measured spatial resolution. Here we use point source scans from a preclinical PET scanner to investigate the relationship between measured spatial resolution and the point source contrast. We also evaluate whether the reconstruction of an isolated point source is predictive of the ability of the system to resolve two adjacent point sources. Our results indicate that when the point source contrast is below a certain threshold, the measured FWHM remains stable. Once the contrast is above the threshold, the measured FWHM monotonically decreases with increasing point source contrast. In addition, the measured FWHM also monotonically decreases with iteration number for maximum likelihood estimate. Therefore, when measuring system resolution with an iterative reconstruction algorithm, we recommend using a low-contrast point source and a fixed number of iterations.

Keywords

positron emission tomography; iterative image reconstruction; spatial resolution

1. Introduction

Positron emission tomography (PET) produces a three dimensional image of the functional processes in the body through the injection of a radioactive tracer. Spatial resolution of PET is an important parameter which has to be accurately measured to achieve the clinical performance in oncology, such as lesion detection (Bal *et al* 2014, Polycarpou *et al* 2014), tumor delineation (Cheebsumon *et al* 2011, Hofheinz *et al* 2013) and therapy monitoring

qi@ucdavis.edu

(Martí-Climent *et al* 2014), neurology (Aguiar *et al* 2008, Mourik *et al* 2010, Bowen *et al* 2013), and cardiology (Mohy-Ud-Din *et al* 2015). Hence when the performance of a PET system is evaluated, measuring the spatial resolution is an important task (Bao *et al* 2009, Visser *et al* 2009, Constantinescu and Mukherjee 2009, Popota *et al* 2012). As recommended by the NEMA standards for both clinical and small animal PET systems (NEMA 2008, 2012), the standard way to characterize the image resolution of a PET system is through point source measurements at different locations. Spatial resolution is measured by reconstructing point source scans using the filtered backprojection (FBP) algorithm and calculating the FWHM from the profiles along the radial and tangential directions. As the FBP algorithm is linear, the measured spatial resolution is independent of any activity distribution in the background. Apart from a point source, other phantoms like a line source (DeGrado *et al* 1994), a cylinder phantom (Lodge *et al* 2009) can also be used to measure the spatial resolution of a PET system.

In recent years, iterative reconstruction algorithms have become the method of choice for PET image reconstruction because of their ability to accurately model the system response and Poisson noise. There is a mismatch between measured point source resolution using the FBP algorithm and real data reconstruction using an iterative method. Furthermore, for system designs that have irregular geometry or missing data, the FBP algorithm cannot be applied without first filling in the missing data (Loukiala *et al* 2010, Tuna *et al* 2010, Goertzen *et al* 2012). These issues make it desirable to measure the achievable spatial resolution of a PET system using an iterative reconstruction algorithm directly. However, measuring spatial resolution for an iterative algorithm can be difficult because the commonly used maximum likelihood (ML) and maximum a posteriori (MAP) reconstruction algorithms for PET are nonlinear and object dependent (Liow and Strother 1993, Yao *et al* 2000). In practical implementations, it has been observed that the non-negativity constraint used in these algorithms can artificially enhance the apparent spatial resolution if a point source image is reconstructed without any background activity (Yang *et al* 2004). It has also been noted that the spatial resolution measured in air is highly dependent on the pixel size and has limitations when being used to evaluate system resolution (Aguiar *et al* 2010, Alessio *et al* 2010). While it has been recommended that a non-zero background be added to the point source data before reconstruction in order to minimize these effects, there has been no detailed study about the effect of the point source contrast level on the measured spatial resolution. As the measured resolution can be contrast dependent, it can result in inconsistent measurements among studies. In addition, due to the nonlinearity of many iterative reconstruction methods, a question may arise about whether the FWHM computed from a single point source truly reflects the system ability to resolve two adjacent points, which is the original definition of spatial resolution (Goodman 2005).

In this work we use point source scans from a preclinical PET scanner in conjunction with maximum-likelihood image reconstruction to investigate: (1) the effect of the point source contrast on the measured spatial resolution, and (2) whether the reconstruction of an isolated point source is predictive of the ability of the system to resolve two adjacent point sources.

2. Methods

2.1. FWHM measurement

A 0.3 mm Na-22 point source encapsulated in Lucite with activity of 132 μCi was scanned in an Inveon preclinical PET scanner (Siemens, Knoxville, TN) at (−15 mm,−15 mm) in the central axial plane as shown in figure 1(a). The crystal size of the Inveon scanner is about 1.59 mm and the 2D sinogram size is 128 (radialbins) × 160 (angles). The total number of events collected in the 2D sinogram was 73 312 and the estimated random fraction was less than 0.1%.

To evaluate the effect of point source contrast on measured spatial resolution, we simulated the background sinogram by forward projecting a uniform background with different activity concentrations using the system matrix, and then superimposed the background projection data onto the point source data before reconstruction. Since the purpose of adding the background is to reduce the nonlinear response and the effect of non-negativity constraint, there is no need to introduce Poisson noise in the background data. Maximum-likelihood image reconstruction was then performed using 5000 iterations of the preconditioned conjugate gradient (PCG) algorithm (Qi *et al* 1998). Only standard normalization was applied in the reconstruction. The system matrix used during forward projection and reconstruction includes a geometric projection matrix and a sinogram blurring matrix (Tohme and Qi 2009). The image matrix size was 1005 × 1005 and the pixel size was 0.1 mm. A small pixel size was used to increase the accuracy of FWHM measurements. Reconstruction of the background sinogram was also performed, and was subtracted from the result of the combined reconstruction to produce the point source only image. Profiles were drawn through the peak of the point source and linear interpolation was performed between neighboring pixels to measure the FWHM along the radial and tangential directions. No curve fitting was performed because the pixel size was much smaller than the expected FWHM. Negative values were not considered in the FWHM calculation. In our implementation, the point source contrast was defined as

$$\text{Contrast}=\frac{\text{Reconstructed point peak intensity}}{\text{Background intensity}}-1 \quad (1)$$

Here the reconstructed point peak intensity refers to the peak intensity of the point source in the reconstructed image before subtracting the background. For comparison, 2D FBP reconstruction using the standard software on the scanner was performed with a pixel size of 0.097 mm. To show the 2D results presented here are applicable to other conditions, fully 3D maximum-likelihood expectation-maximization (MLEM) reconstruction of a point source at the center of the FOV was also performed with different background values. The image matrix size in the 3D reconstruction was 256 × 256 × 161 with a voxel size of 0.194 × 0.194 × 0.796 mm^3.

2.2. Resolvability of adjacent points

The second goal of this study is to determine whether the reconstruction of an isolated point source can be used to predict the ability of the system to resolve two adjacent hot spots. In order to do this, we scanned the point source at two additional positions, one at (−16 mm,

−14 mm) and the other at (−14 mm, −14 mm), as shown in figure 1(b). These two new point sources are separated from the original point source by 1.4 mm, the former in the tangential direction and the latter in the radial direction. For each pair of point sources, we reconstructed images generated from two different methods of combination: (1) reconstruct the two point sources independently and then combine them together in the image space; and (2) combine the point source sinograms and reconstruct the two point sources together. For both methods, sinograms were reconstructed after adding different level of background values. To quantify the difference between the two reconstruction methods, the valley-to-peak ratio (VPR) of the two point sources was measured for comparison.

3. Results

3.1. FWHM measurement

Figure 2 shows the tangential FWHM as a function of point source contrast at different numbers of iterations. This figure presents an overview of the influence of contrast and iteration number on the FWHM measurement. First, we see that the FWHM decreases with increasing number of iterations. Second, at a fixed iteration, the FWHM increases with decreasing contrast, then remains stable after a certain threshold is reached. To better visualize this trend, figure 3(a) plots the FWHM at iteration 5000 for different contrast levels. It can be seen from this figure that when the contrast is below 0.1 (i.e., $\log_{10}$ (contrast)< −1), the FWHM remains stable. This phenomenon is also evident when looking at the reconstructed point source images of different contrasts shown in figure 4. These findings tell us that without adding a background to the point source, the measured FWHM is much lower than the measured FWHM with a background. For example, when the contrast is 1000 (similar to the no background case), as shown in figure 3(a), the measured FWHM is 0.2 mm, much smaller than the resolution obtained at a lower contrast. Thus the FWHM measured without background is often unrealistic. Similar trend was also observed for the FWHM measurement from the fully 3D ML EM reconstruction as shown in figure 3(b), indicating that the findings are applicable to other imaging situations. For comparison, the 2D FBP reconstruction is shown in figure 4(e). The measured radial FWHM is 2.17 mm and the tangential FWHM is 1.67 mm, both of which match the previous published values at the radial offset of 21 mm (Bao *et al* 2009, Constantinescu and Mukherjee 2009, Visser *et al* 2009).

3.2. Resolvability of adjacent points

Figure 5 compares the sum of individual reconstructions (top row) and the reconstructions of the summed sinogram (bottom row) at three contrast levels for the tangentially separated point sources. Tangential profiles for the cases with the two background levels are shown in figure 6. From the images and the profiles we can see that only when the contrast is low, the summed reconstruction of individual point sources is similar to the reconstruction of the summed sinogram. To quantify the difference between the two reconstructions, we calculated the VPR and plot them in figure 7. We can see that at high contrast level, the summed image has a lower VPR than the reconstruction of the summed sinogram, indicating that the point source resolution overestimates the system ability to resolve two adjacent hot spots. At lower contrast levels, both images achieve similar VPR, so the reconstructed point

source image is a good prediction of the system ability to resolve two adjacent hot spots. This means that the measured FWHM at low contrast can tell the system's ability to distinguish small objects while at high contrast it cannot. Additionally, we see that the threshold (about 0.1) below which both images achieve similar VPR is the same as the threshold below which the FWHM remains stable. Hence when the contrast is below a threshold (about 0.1) the measured FWHM is indicative of the resolvability of the system.

3.3. Effect of resolution modeling

In the above studies, a sinogram domain blurring matrix was used to model the detector response. Here we examine the effect of the resolution modeling on resolution measurement by comparing the reconstruction results with and without the blurring matrix. Both the MLEM and PCG algorithms were studied. The FWHM values measured at 500 iteration and 5000 iteration are shown in figure 8. It is interesting to see that at 500 iteration the FWHM with the blurring matrix can be worse than that without the blurring matrix for a low-contrast point source. The trend is the same for PCG and MLEM, although MLEM requires a higher contrast to realize the resolution improvement by resolution modeling because it converges slower than PCG. The reason for this seemingly counter-intuitive result is that resolution modeling makes the system equation more ill-conditioned, which slows down the convergence speed of both the PCG and MLEM algorithms. Therefore, the benefit of resolution model at early iterations is not improvement of spatial resolution, but reduction of noise. At 5000 iteration, we see that both algorithms provide consistently better FWHM with the sinogram blurring matrix than without the blurring matrix across all contrast levels, which is consistent with the expectation.

4. Discussion

Our study has shown that the measured FWHM of an iterative reconstruction algorithm can be greatly influenced by the point source contrast and number of iterations. In particular, at high contrast (or no background) the measured FWHM has the potential to be rendered meaningless as it can approach the voxel size at a very large number of iterations. Also, for high contrast cases, the measured system FWHM cannot represent the system's ability to distinguish two objects. We note that apart from the non-negativity constraint, the nonlinearity of the iterative methods used here is another factor that causes contrast-dependent resolution. This can be seen from the point spread functions in figures 4(b)-(d). In all three cases, the added background value is large enough to make the elements in the iterative update equation all be positive, but we still obtained different FWHM values. While non-negativity constraint can be removed from reconstruction algorithms, nonlinearity is inherent to the Poisson likelihood function and cannot be avoided in statistically based PET reconstruction. The same applies to (penalized) weighted least squares (WLS) reconstructions in which the weights are data dependent (Fessler 1994). While there are linear iterative algorithms based on the least squares, such as ART, they are not commonly used for PET reconstruction because they result in higher noise in reconstructed images. Therefore, it is important to use a low-contrast point source embedded in a background when measuring spatial resolution using an statistically based iterative reconstruction method. While the measured FWHM may be larger than that of a source with a higher

contrast, the result provides a lower bound of the system resolvability that can be used to compare different PET scanners. In real applications, a look-up table (e.g. figure 2) can be provided to estimate the extent of spatial blurring for a given hot spot based on its contrast and the specific reconstruction algorithm. For applications that require a contrast-independent resolution, one may have to use a linear algorithm with sacrifice in noise.

The results in figure 3 show that the contrast threshold of 0.1 holds for both 2D reconstruction with 0.1 mm pixels and 3D reconstruction with larger voxels. These voxel sizes are consistent with the NEMA standard (NEMA 2012), which recommends using voxel size no more than one third of the expected FWHM in all three dimensions for resolution measurements. As an extreme case, we also performed reconstructions with 0.5 mm pixels (data not shown) and found the same threshold. Therefore, the threshold appears to be independent of the voxel size as long as it is less than one third of the expected FWHM.

5. Conclusion

In this work, we have studied the dependence of measured spatial resolution on point source contrast and system modeling. To minimize the variation in the measured FWHM value for system performance evaluation, we recommend that the reconstructed point source contrast should be lower than 0.1, i.e. the reconstructed peak intensity of the point source with background should be less than 110% of the background activity, based on the results in this study. In addition, because the measured FWHM depends on the reconstruction algorithm and number of iterations, it is also important to use the same algorithm and same number of iterations when comparing different systems.

Acknowledgments

We would like to thank the anonymous reviewers for their helpful suggestions. This work was supported by the National Institutes of Health under grant number R01EB000194.

References

Aguiar P, Pareto D, Gispert J, Crespo C, Falcon C, Cot A, Lomeña F, Pavía J, Ros D. Effect of anatomical variability, reconstruction algorithms and scattered photons on the SPM output of brain PET studies. Neuroimage. 2008; 39:1121–8. [PubMed: 18042402]

Aguiar P, Rafecas M, Ortuño JE, Kontaxakis G, Santos A, Pavía J, Ros D. Geometrical and Monte Carlo projectors in 3D PET reconstruction. Med. Phys. 2010; 37:5691–702. [PubMed: 21158281]

Alessio AM, Stearns CW, Tong S, Ross SG, Kohlmyer S, Ganin A, Kinahan PE. Application and evaluation of a measured spatially variant system model for PET image reconstruction. IEEE Trans. Med. Imaging. 2010; 29:938–49. [PubMed: 20199927]

Bal H, Guerin L, Casey M, Conti M, Eriksson L, Michel C, Fanti S, Pettinato C, Adler S, Choyke P. Improving PET spatial resolution and detectability for prostate cancer imaging. Phys. Med. Biol. 2014; 59:4411–26. [PubMed: 25049221]

Bao Q, Newport D, Chen M, Stout DB, Chatziioannou AF. Performance evaluation of the inveon dedicated PET preclinical tomograph based on the NEMA NU-4 standards. J. Nucl. Med. 2009; 50:401–8. [PubMed: 19223424]

Bowen SL, Byars LG, Michel CJ, Chonde DB, Catana C. Influence of the partial volume correction method on 18f-fluorodeoxyglucose brain kinetic modelling from dynamic PET images

reconstructed with resolution model based osem. Phys. Med. Biol. 2013; 58:7081–106. [PubMed: 24052021]

Cheebsumon P, van Velden FH, Yaqub M, Frings V, de Langen AJ, Hoekstra OS, Lammertsma AA, Boellaard R. Effects of image characteristics on performance of tumor delineation methods: a test–retest assessment. J. Nucl. Med. 2011; 52:1550–8. [PubMed: 21849398]

Constantinescu CC, Mukherjee J. Performance evaluation of an inveon PET preclinical scanner. Phys. Med. Biol. 2009; 54:2885. [PubMed: 19384008]

DeGrado TR, Turkington TG, Williams JJ, Stearns CW, Hoffman JM, Coleman RE. Performance characteristics of a whole-body PET scanner. J. Nucl. Med. 1994; 35:1398–406. [PubMed: 8046501]

Fessler JA. Penalized weighted least-squares image reconstruction for PET. IEEE Trans. Med. Imaging. 1994; 13:290–300. [PubMed: 18218505]

Goertzen AL, et al. NEMA NU 4-2008 comparison of preclinical PET imaging systems. J. Nucl. Med. 2012; 53:1300–9. [PubMed: 22699999]

Goodman, JW. Introduction to Fourier Optics. Roberts and Company; Greenwood Village, CO: 2005.

Hofheinz F, Langner J, Petr J, Beuthien-Baumann B, Steinbach J, Kotzerke J, van den Hoff J. An automatic method for accurate volume delineation of heterogeneous tumors in PET. Med. Phys. 2013; 40:082503. [PubMed: 23927348]

Liow JS, Strother S. The convergence of object dependent resolution in maximum likelihood based tomographic image reconstruction. Phys. Med. Biol. 1993; 38:55–70. [PubMed: 8426869]

Lodge MA, Rahmim A, Wahl RL. A practical, automated quality assurance method for measuring spatial resolution in PET. J. Nucl. Med. 2009; 50:1307–14. [PubMed: 19617324]

Loukiala A, Tuna U, Beer S, Jahnke S, Ruotsalainen U. Gap-filling methods for 3D PlanTIS data. Phys. Med. Biol. 2010; 55:6125–40. [PubMed: 20871138]

Martí-Climent JM, Prieto E, Elosúa C, Rodríguez-Fraile M, Domínguez-Prado I, Vigil C, García-Velloso MJ, Arbizu J, Peñuelas I, Richter JA. PET optimization for improved assessment and accurate quantification of 90Y-microsphere biodistribution after radioembolization. Med. Phys. 2014; 41:092503. [PubMed: 25186412]

Mohy-Ud-Din H, Lodge MA, Rahmim A. Quantitative myocardial perfusion PET parametric imaging at the voxel-level. Phys. Med. Biol. 2015; 60:6013–38. [PubMed: 26216052]

Mourik JE, Lubberink M, Van Velden FH, Kloet RW, Van Berckel BN, Lammertsma AA, Boellaard R. *In vivo* validation of reconstruction-based resolution recovery for human brain studies. J. Cerebral Blood Flow Metabolism. 2010; 30:381–89.

National Electrical Manufacturers Association. Performance measurements of small animal positron emission tomographs NEMA Standards Publication NU 4-2008. National Electrical Manufacturers Association; Rosslyn, VA: 2008.

National Electrical Manufacturers Association. Performance measurements of positron emission tomographs NEMA Standards Publication NU 2-2012. National Electrical Manufacturers Association; Rosslyn, VA: 2012.

Polycarpou I, Tsoumpas C, King AP, Marsden PK. Impact of respiratory motion correction and spatial resolution on lesion detection in PET: a simulation study based on real MR dynamic data. Phys. Med. Biol. 2014; 59:697–714. [PubMed: 24442386]

Popota FD, Aguiar P, Herance JR, Pareto D, Rojas S, Ros D, Pavía J, Gispert JD. Comparison of the performance evaluation of the microPET R4 scanner according to NEMA standards NU 4-2008 and NU 2-2001. IEEE Trans. Nucl. Sci. 2012; 59:1879–86.

Qi J, Leahy RM, Hsu C, Farquhar TH, Cherry SR. Fully 3D bayesian image reconstruction for the ECAT EXACT HR + IEEE Trans. Nucl. Sci. 1998; 45:1096–103.

Tohme MS, Qi J. Iterative image reconstruction for positron emission tomography based on a detector response function estimated from point source measurements. Phys. Med. Biol. 2009; 54:3709–26. [PubMed: 19478379]

Tuna U, Peltonen S, Ruotsalainen U. Gap-filling for the high-resolution PET sinograms with a dedicated DCT-domain filter. IEEE Trans. Med. Imaging. 2010; 29:830–9. [PubMed: 20199918]

Visser EP, Disselhorst JA, Brom M, Laverman P, Gotthardt M, Oyen WJ, Boerman OC. Spatial resolution and sensitivity of the inveon small-animal PET scanner. J. Nucl. Med. 2009; 50:139–47. [PubMed: 19139188]

Yang Y, Tai YC, Siegel S, Newport DF, Bai B, Li Q, Leahy RM, Cherry SR. Optimization and performance evaluation of the microPET II scanner for *in vivo* small-animal imaging. Phys. Med. Biol. 2004; 49:2527–46. [PubMed: 15272672]

Yao R, et al. Performance characteristics of the 3-D OSEM algorithm in the reconstruction of small animal PET images. IEEE Trans. Med. Imaging. 2000; 19:798–804. [PubMed: 11055803]

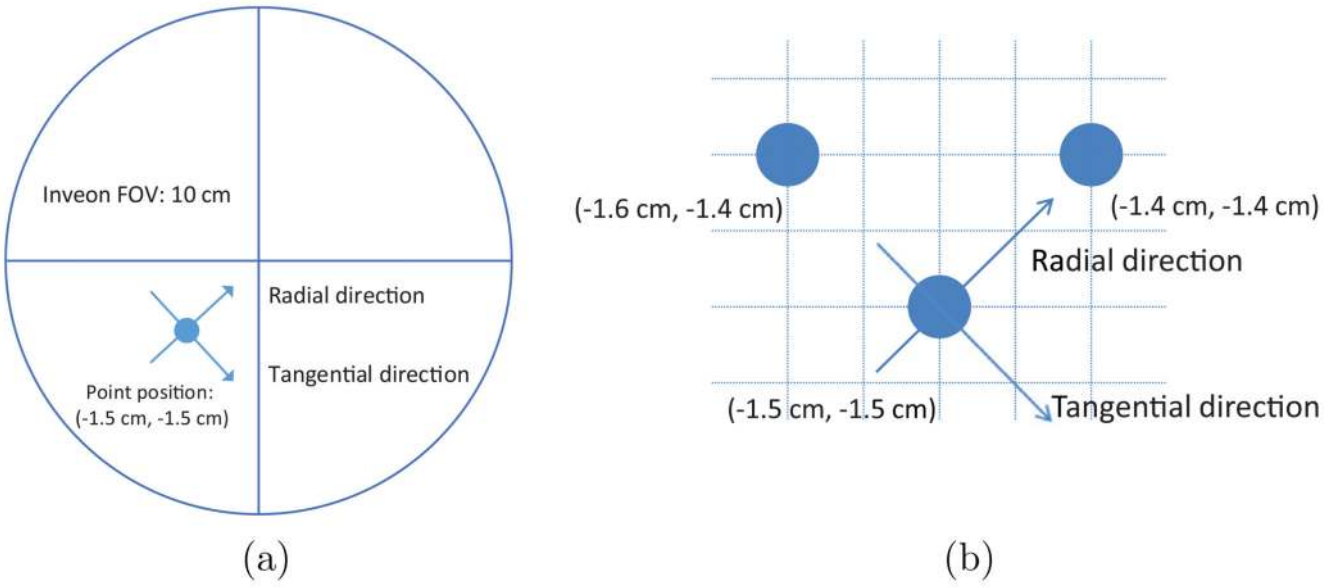

Figure 1.

(a) The location of the point source that was used to measure the FWHM. (b) The location of the point source pairs in the radial and the tangential directions.

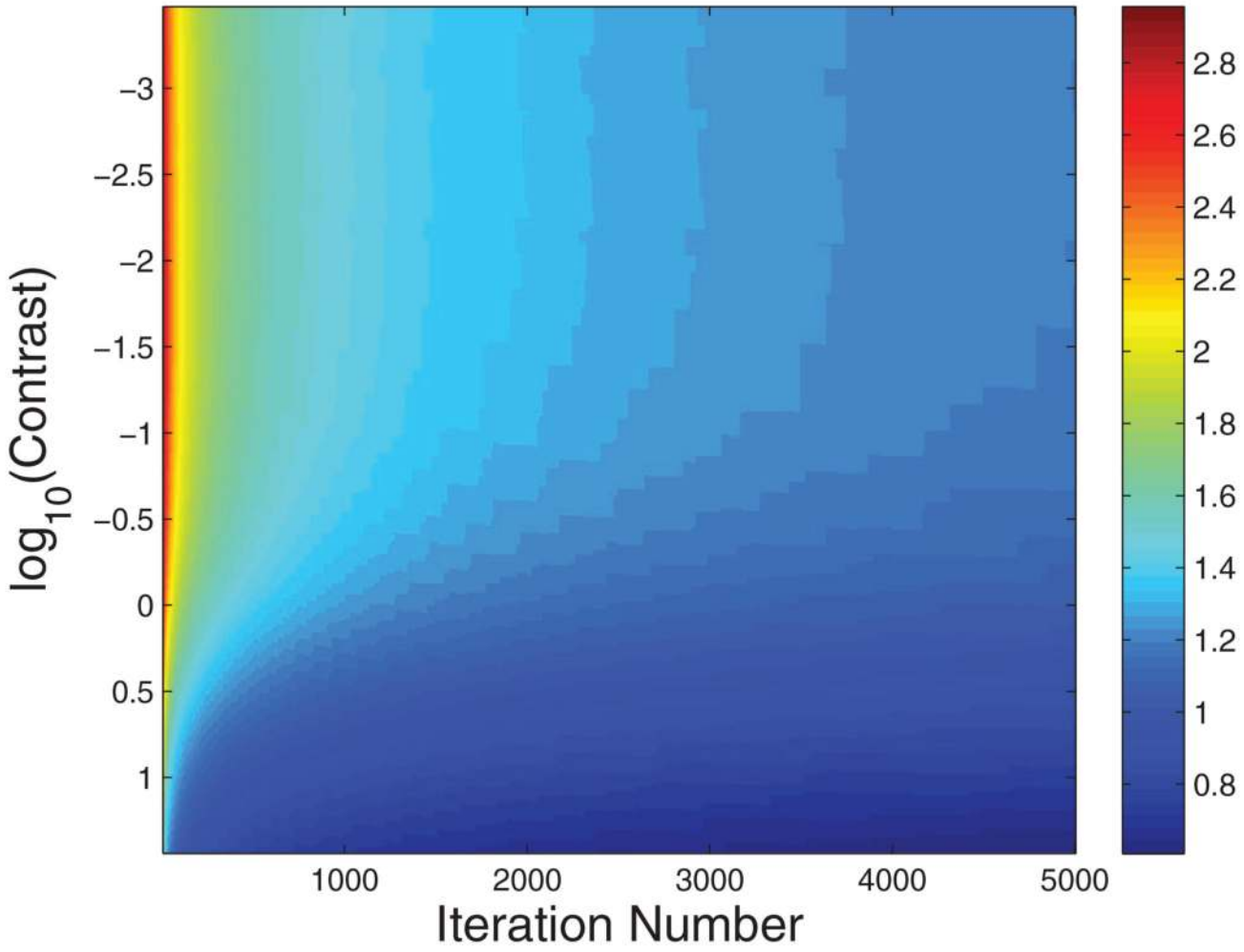

Figure 2.
The measured tangential FWHM at different contrast levels and different number of iterations using PCG algorithm.

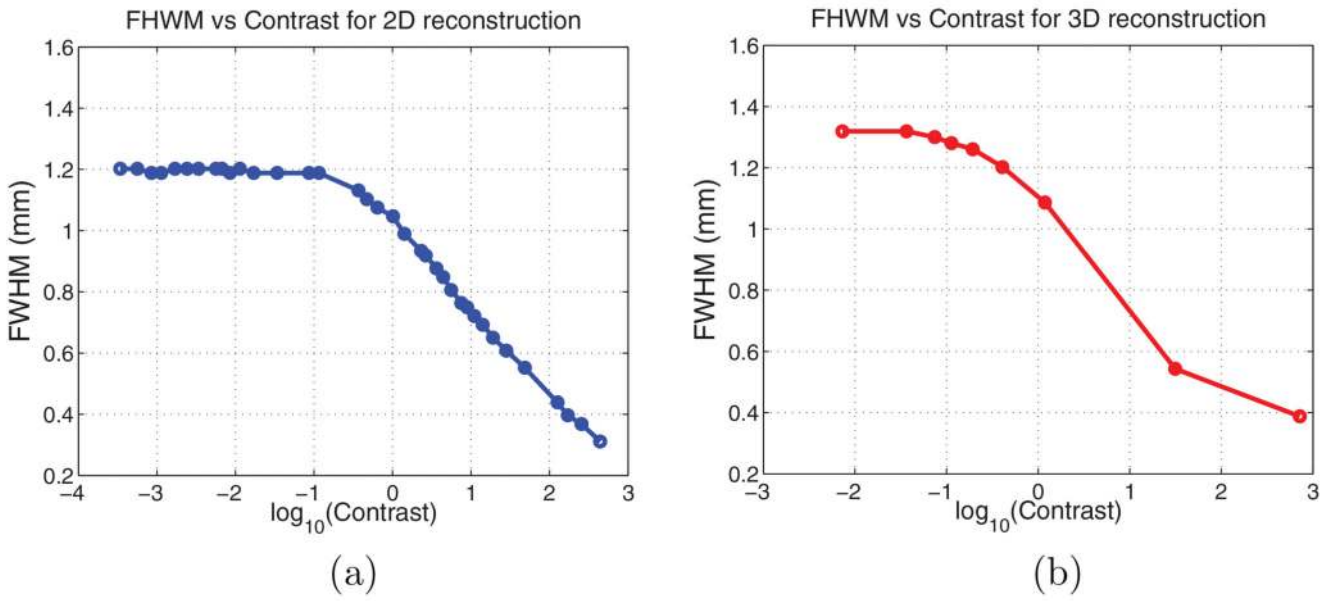

Figure 3.

(a) The measured tangential FWHM at different contrast levels for 2D reconstruction using 5000 iterations of the PCG algorithm. (b) The measured tangential FWHM at different contrast levels for 3D reconstruction of a point source at the center using 500 iterations of the MLEM algorithm.

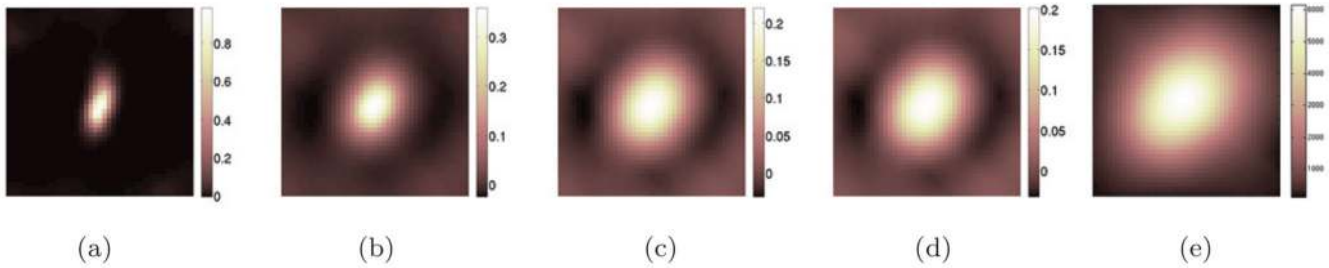

Figure 4.

The reconstructed point source image at iteration 5000 with different contrast (C) levels: (a) $C = 196$, (b) $C = 7.2$, (c) $C = 0.44$, (d) $C = 0.04$. The 2D FBP reconstruction is shown in (e). The physical size of each image patch is 4.2 mm × 4.2 mm. Each colormap is scaled to range from the minimum to the maximum of the respective image.

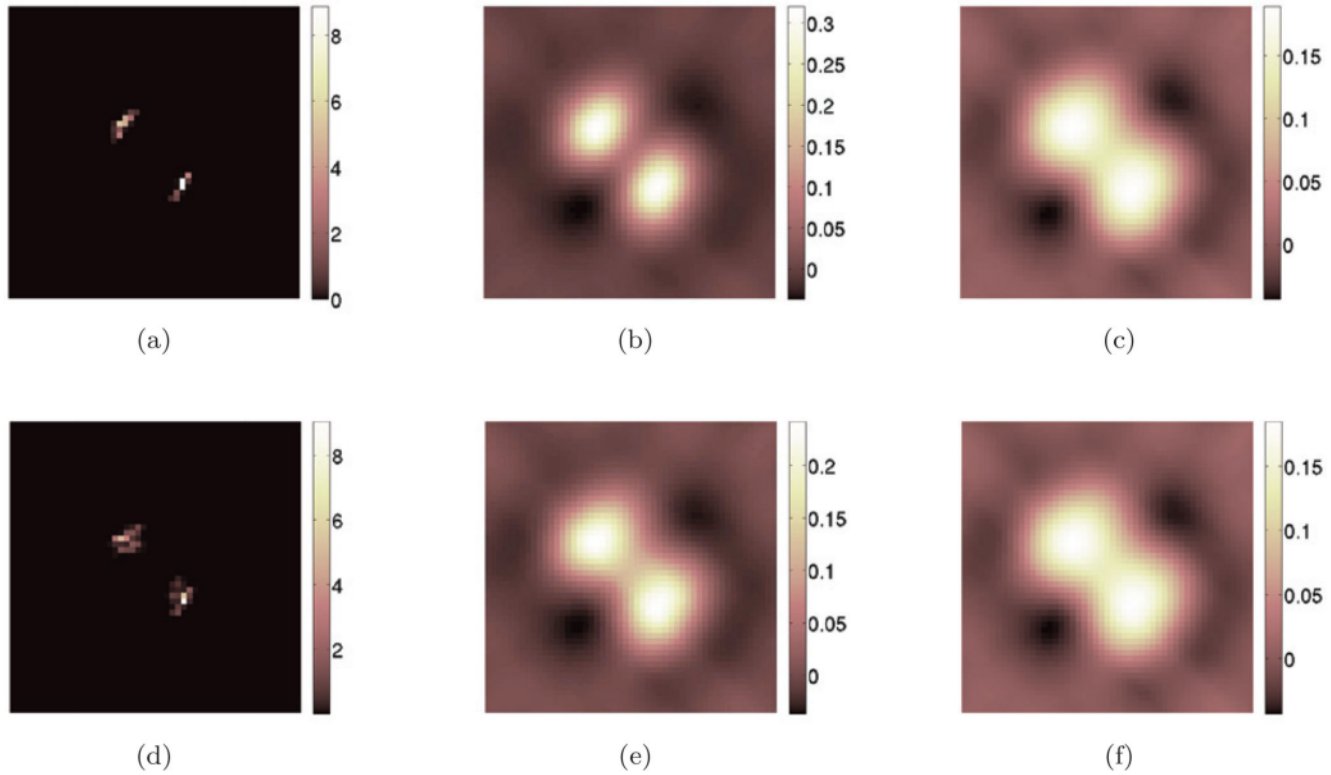

Figure 5.

The sum of individual reconstructions (top row) and the reconstructions of the summed sinograms (bottom row) at three contrast levels. The two points are separated by 1.4 mm tangentially. (a) Background = 0. (b) Background = 0.064. (c) Background = 2.0. (d) Background = 0. (e) Background = 0.064. (f) Background = 2.0.

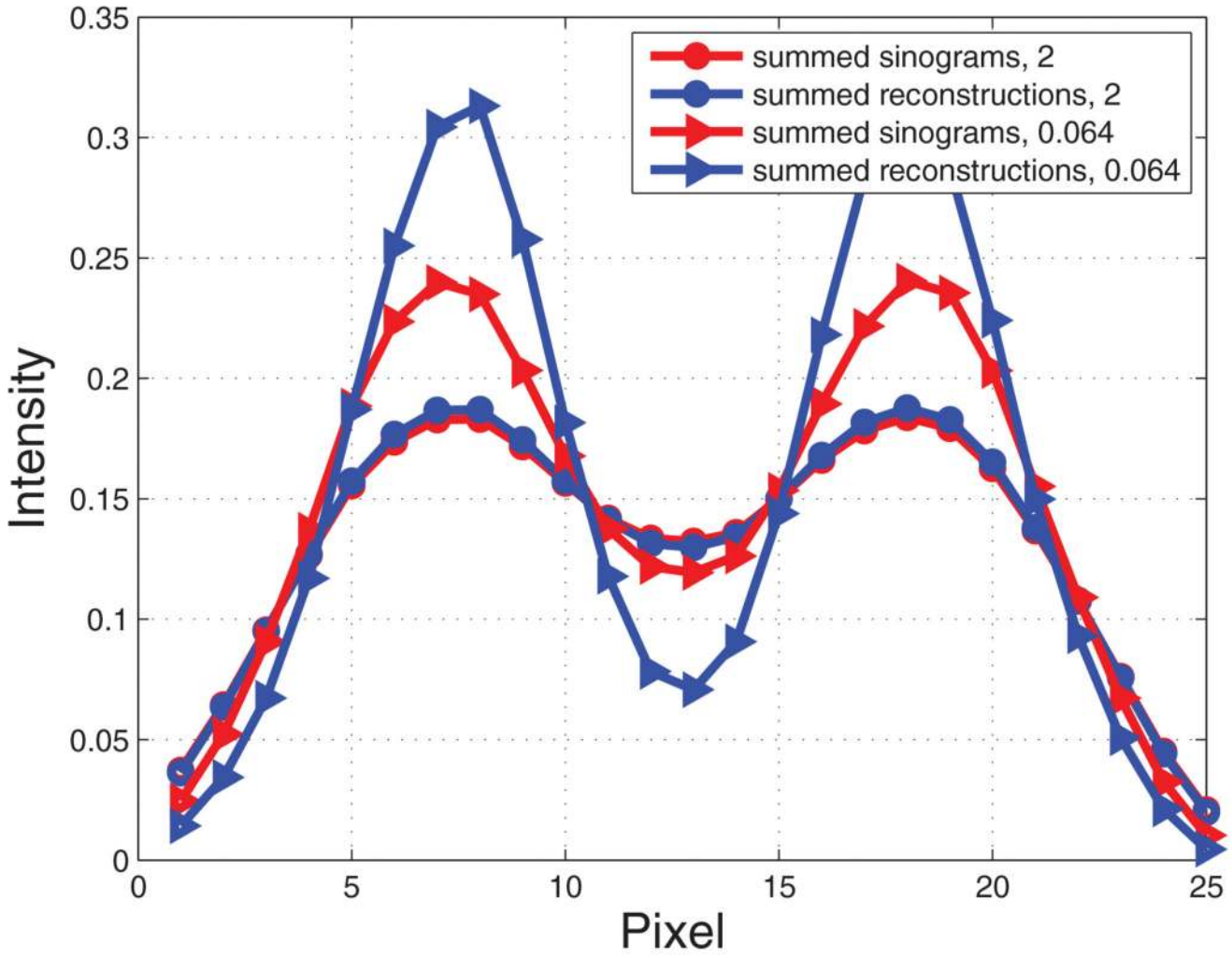

Figure 6.
Tangential profiles through the reconstructed images in figure 5. The numbers in the legend correspond to the background values.

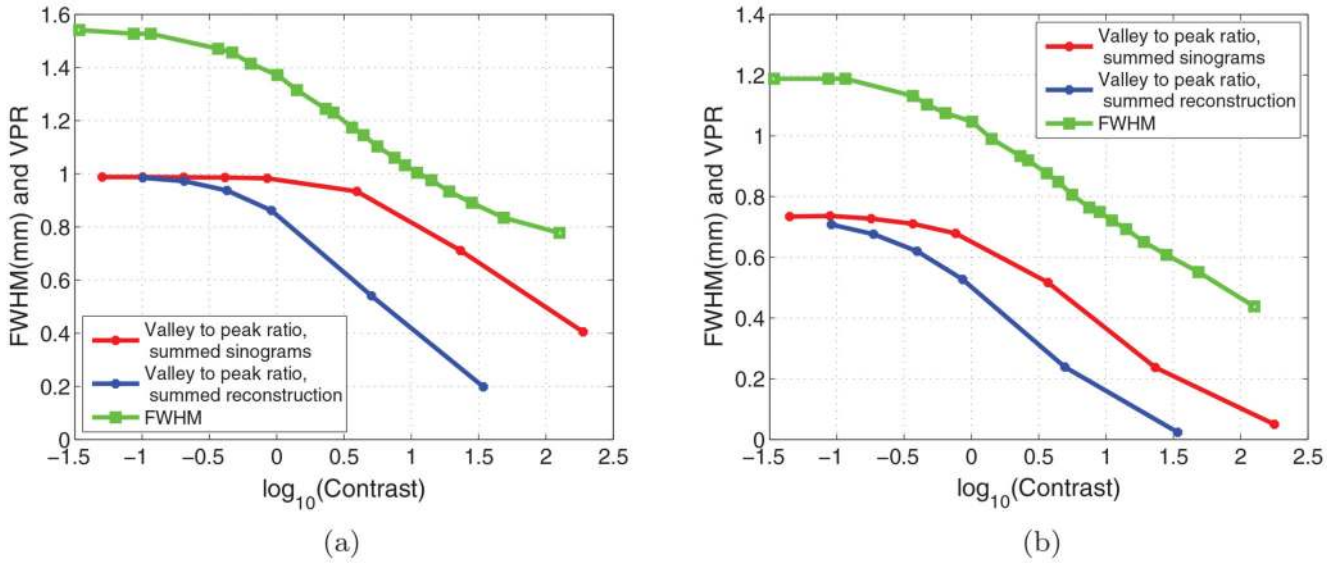

Figure 7.

Comparison of the valley-to-peak ratio (VPR) between the summed reconstructions and reconstruction of the summed sinograms: (a) radial direction and (b) tangential direction. The measured FWHM values are also shown.

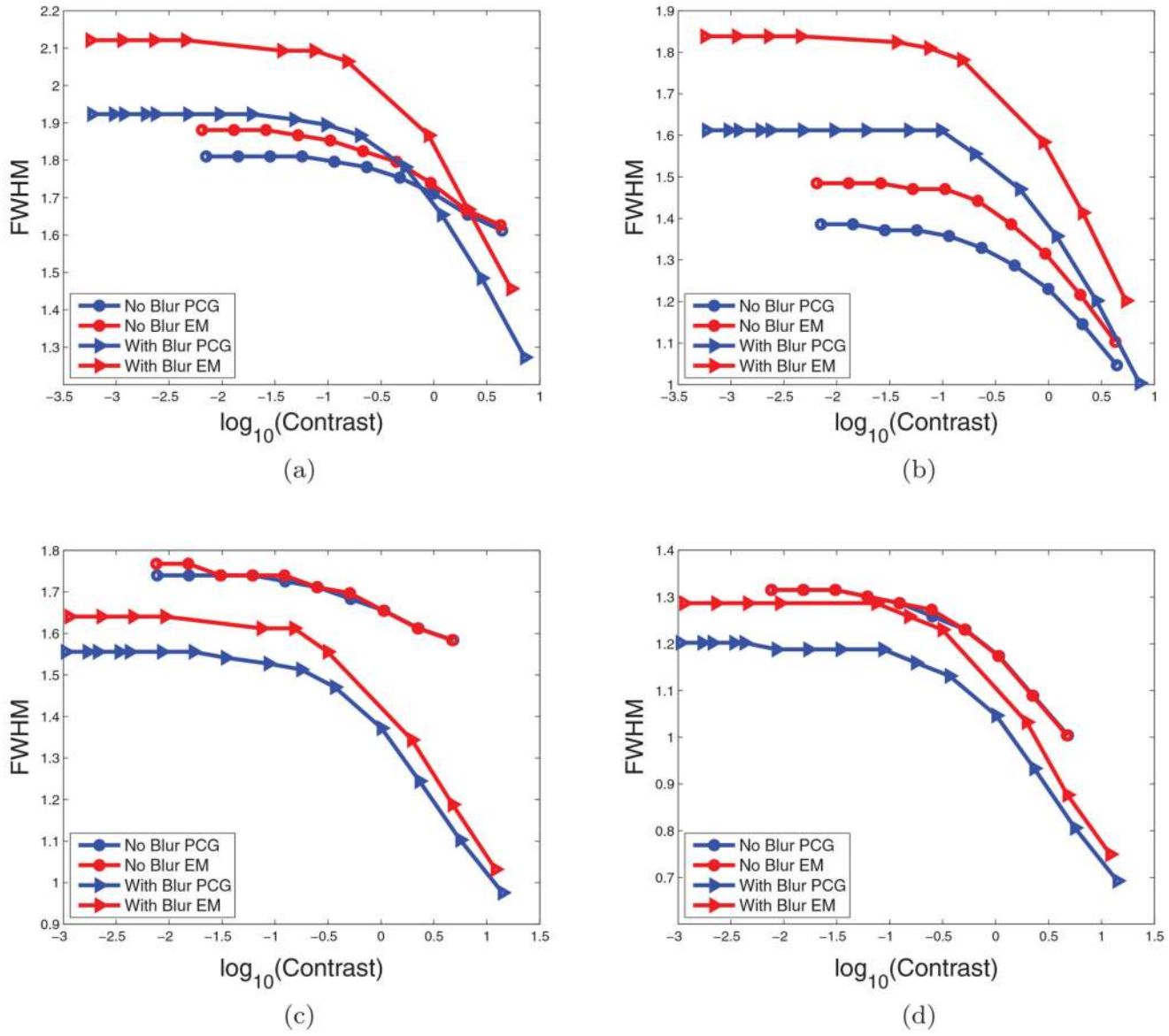

Figure 8.

Comparison between reconstructions with and without the blurring matrix. Results of both the PCG and MLEM algorithm are shown. (a) Iteration 500, Radial. (b) Iteration 500, Tangential. (c) Iteration 5000, Radial. (d) Iteration 5000, Tangential.